Solar Energy Materials & Solar Cells 94 (2010) 2073–2077

Contents lists available at ScienceDirect

Solar Energy Materials & Solar Cells

journal homepage: www.elsevier.com/locate/solmat

A method to measure resistivity, mobility, and absorber thickness in thin-film solar cells with application to CdTe devices

Jian V. Li*, Xiaonan Li, David S. Albin, Dean H. Levi

National Renewable Energy Laboratory, Golden, CO 80401, USA

ARTICLE INFO

Article history:
Received 17 March 2010
Received in revised form
21 May 2010
Accepted 21 June 2010

Keywords:
Admittance spectroscopy
Capacitance–voltage
Mobility
Absorber thickness
CdTe
Back contact

ABSTRACT

We report a method developed upon coordinated admittance spectroscopy and capacitance–voltage techniques to measure resistivity, mobility, and absorber thickness in thin-film photovoltaic devices. The absorber thickness is measured by depletion region width at freeze-out temperatures when the free carriers cease to respond to bias modulation. Based on a lumped-parameter equivalent-circuit model, we derive the inflection frequency due to dielectric relaxation of the absorber. We show that the square of freeze-out frequency depends linearly on bias voltage. Resistivity—and mobility—is calculated from the slope of this linear dependence. To demonstrate this method, we applied it to thin-film CdTe solar cells with back contacts formed under three different conditions: (A) with Cu in the carbon paste after nitric–phosphoric etch, (B) without Cu in the carbon paste after nitric–phosphoric etch, and (C) without Cu in the carbon paste and without nitric–phosphoric etch. The measured absorber thicknesses (5.45, 5.85, and 7.95 μm, respectively) agree well with growth history and other methods. Study using this method also yields insights to back-contact formation mechanism in terms of etching loss, Te-rich layer, and Cu doping/alloying. The freeze-out exhibits thermal activation due to combined contribution from mobility and carrier concentration.

1. Introduction

Thin-film solar cells are important photovoltaic devices for harvesting solar energy. Current major technologies are CdTe, $Cu(InGa)Se_2$, amorphous silicon, and organic materials. The absorbers in these devices are typically of direct bandgap, thin, and non-monocrystalline in nature. This work is concerned with two aspects of the absorber layer: (1) its majority charge transport represented by resistivity and mobility, and their temperature dependence and (2) averaged thickness of the portion that is electrically active. The resistivity and mobility of the absorber are important to the performance of the solar cell because they affect series resistance and photo-carrier collection. They are typically much lower than those in monocrystalline material. For certain materials, e.g., CdTe, the low mobility together with low free-carrier concentration introduces difficulty in the standard Hall measurement and leads to a general lack of resistivity/mobility data. On the other hand, absorber thickness and uniformity not only influence the device performance but are also directly related to the manufacturing cost and yield. It depends on both film deposition conditions (such as substrate temperature and time) and device processing conditions (such as chemical etch and contact formation). Absorber thickness in a finished device closely reflects the formation processes of the two boundaries of the absorber, e.g., the hetero-interface to CdS and the back contact in the case of CdTe, which are among the most critical issues in understanding and improving device performance. Depending on the particular material and technology, the accurate measurement of absorber thickness and its electrical properties can be elusive. Thus, there is an immediate need for a reliable method to measure low resistivity, mobility, and thickness of various thin-film absorber materials.

From a methodological and practical point of view, it is desirable to measure resistivity, mobility, and absorber thickness in a finished solar cell device—as opposed to those at the material level (e.g., required by the Hall technique) in the early stage of device fabrication or in a device specially designed for specific techniques such as time-of-flight. The obvious reason is that the properties to be measured are sensitive to processing steps and in an actual solar cell they may be different from those in a specially grown material or specially structured device. The freeze-out phenomenon has been used to study amorphous silicon devices [1]. Recently, Lee et al. [2] reported determining the mobility in a $Cu(In,Ga)Se_2$ device using high-frequency admittance measurements. In this work, we elaborate on the previous methods to measure averaged "electrically active thickness," resistivity, and majority-carrier mobility of a lightly doped thin-film absorber from coordinated capacitance–voltage

* Corresponding author.
E-mail address: jian.li@nrel.gov (J.V. Li).

0927-0248/$ - see front matter © 2010 Elsevier B.V. All rights reserved.
doi:10.1016/j.solmat.2010.06.018

and admittance spectroscopy measurements. We apply this method to CdTe thin-film solar cells to demonstrate its validity. The results obtained using this method lead to physical insights on the mechanism of back-contact formation in terms of pre-contact etching effect, formation of Te-rich layer, and the effect of incorporating Cu in the back-contact material.

2. Method

Lee et al. [2] described an equivalent circuit of the absorber using a distributed parameter (transmission line) model for the semi-neutral region. In Fig. 1, we describe a lumped-parameter equivalent circuit that is simpler and more intuitive. A semiconductor characterized by resistivity ρ and permittivity ε exhibits dielectric relaxation at frequency $\omega_{dr}=1/\rho\varepsilon$. Below ω_{dr}, the semiconductor behaves like a conductor with $G_g=A/\rho t$, where A is the area and t the thickness. Above ω_{dr}, the semiconductor behaves like a capacitor $C_g=\varepsilon A/t$, where ε is the permittivity. Therefore, one can model the equivalent circuit of the semi-neutral portion of the absorber as the parallel connection of G_g and C_g. In a typical n^+/p solar cell device, the equivalent-circuit model becomes the series connection of a depletion capacitance C_d determined by the depletion region width W, and that of the semi-neutral absorber described above. As to the total capacitance C and conductance G, our model arrives at the same frequency dependence as that by Lee et al. [2]. The frequency dependence of the total capacitance C is as follows:

$$C = C_d \frac{\omega^2\rho^2\varepsilon^2 C_d/C_g + 1}{\omega^2\rho^2\varepsilon^2 C_d^2/C_g^2 + 1}. \tag{1}$$

The capacitance C vs frequency ω plot thus exhibits a step transition around an inflection point ω_p, below which C approaches C_d and above which C approaches C_g. The step transition in the C vs ω curve is transformed to a minimum in the differential capacitance $\omega\, dC/d\omega$ vs ω curve, from which the inflection frequency is easier to identify. We arrive at the differential capacitance $\omega\, dC/d\omega$ and inflection frequency ω_p by taking the numerical derivative of C with respect to ω:

$$\omega\frac{dC}{d\omega} = C_d \frac{2(1-C_d/C_g)\omega^2\rho^2\varepsilon^2 C_d/C_g}{\left[\omega^2\rho^2\varepsilon^2 C_d^2/C_g^2 + 1\right]^2}. \tag{2}$$

$$\omega_p = \frac{C_g}{C_d\rho\varepsilon} = \frac{W}{t}\frac{1}{\rho\varepsilon}. \tag{3}$$

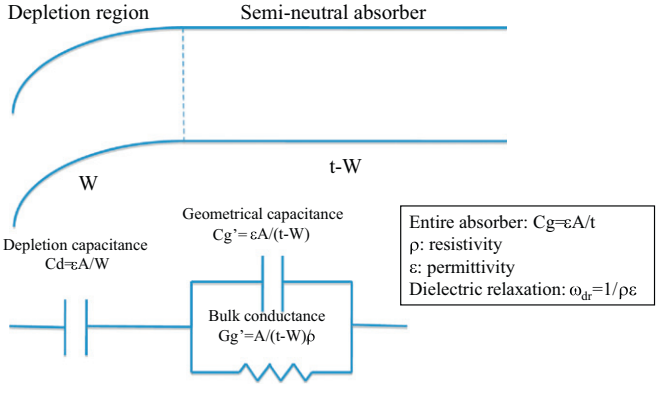

Fig. 1. Band structure (a) and equivalent-circuit model (b) for the absorber (thickness t) in a typical thin-film solar cell device. The depletion region (depletion width W) is modeled as depletion capacitance C_d. The semi-neutral region is modeled as the parallel connection of lump-parameter geometrical capacitance C'_g and conductance G'_g.

On the other hand, the total conductance G shows similar dispersion behavior as the differential capacitance, i.e., G/ω exhibits a peak at ω_p. There are three unknowns in Eqs. (2) and (3): C_d (or W), C_g (or t), and ρ. Lee et al. [2] determine C_d, C_g, and ρ from the experimental C vs ω data using multivariable fitting according to Eq. (2). In this work, we take advantage of the voltage dependence of freeze-out frequency to extract resistivity ρ and mobility μ from film thickness t and carrier concentration N_a measured by capacitance–voltage and admittance spectroscopy techniques.

We first measure t from the depletion width at low temperatures, where full depletion of the absorber occurs because the carriers can no longer respond to voltage modulation at frequencies higher than ω_{dr}. The electrically active absorber thickness t equals $\varepsilon A/C$. For a perfectly uniform and planar device, assuming carrier density in the n^+ and back-contact layers are infinite, t is exactly the absorber thickness. In an actual thin-film device, this is an averaged value of a large area containing many grains, and it may contain small errors due to the finite depletion region extending to the n^+ and contact layers. We assume the absorber freezes out before the n^+ and contact layers.

We then use the bias dependence of inflection frequency ω_p to determine resistivity ρ and mobility μ. Since the depletion region width for an n^+–p junction is

$$W = \sqrt{\frac{2\varepsilon}{qN_a}(V_{bi}-V)},$$

we arrive at the following expression for the square of inflection frequency:

$$\omega_p^2 = \frac{W^2}{t^2}\frac{1}{\rho^2\varepsilon^2} = \frac{2}{q\varepsilon N_a\rho^2 t^2}(V_{bi}-V). \tag{4}$$

It is obvious that ω_p exhibits a non-linear redshift as V increases toward the forward bias. However, the square of inflection frequency ω_p^2 has a linear dependence on bias voltage V. If one plots ω_p^2 against bias V, the slope of this plot can be used to determine resistivity:

$$\rho = \sqrt{\frac{2}{q\varepsilon N_a t^2\, slope}}, \tag{5}$$

or equivalently, mobility:

$$\mu = \frac{1}{qN_a\rho} = \sqrt{\frac{\varepsilon t^2\, slope}{2qN_a}}, \tag{6}$$

where the carrier concentration N_a is determined from capacitance–voltage measurements.

3. Experimental and material

We use an Agilent 4294 impedance analyzer to measure the capacitance–voltage and admittance raw data. Unless otherwise specified, frequency is set at 10 kHz for capacitance–voltage measurements and ac modulation amplitude is 45 mV_{p-p}. For the admittance spectroscopy experiment, frequency and temperature are varied from 10^3 to 10^6 Hz and 50 to 330 K, respectively. A silicon-diode temperature sensor is attached to the top of the device to reduce error in temperature readings due to the large thermal gradient caused by the glass substrate.

The thin-film CdTe solar cells were fabricated with nominally the same procedure as described in Ref. [3]. First, a layer of transparent conductive oxide was grown on the glass substrate. Then, a layer of CdS was grown using chemical-bath deposition, followed by the growth of the CdTe thin film with close-spaced

sublimation. To this point, all samples were fabricated the same way; the difference is in the next two processing steps that form the back contact. The standard procedure calls for an etching step in nitric–phosphoric acid, followed by applying a carbon paste back-contact layer containing Cu. To vary the electrically active CdTe film thickness, we used three different conditions: (A) with Cu after nitric–phosphoric etch (labeled Cu/NP), (B) without Cu after nitric–phosphoric etch (labeled X/NP), and (C) neither Cu nor nitric–phosphoric etch (labeled X/X). Except for the back-contact formation process, all devices are nominally identical. All three types of back contacts were completed with carbon paste, in which Cu is either present (type A: Cu/NP) or absent (type B: X/NP and type C: X/X).

4. Results

Using standard procedures applicable to an abrupt one-sided junction, we calculate the carrier concentration N_a from the local slope of the Mott–Schottky plot of C^{-2} vs bias $N_a = -2/slope/q\varepsilon A^2$ and depletion region $W = \varepsilon A/C$. We first look at the temperature dependence of carrier concentration N_a and depletion region width W taken from the type A (Cu/NP) sample at zero bias and 10 kHz, as shown in Fig. 2. Based on the behavior of N_a and W, four temperature zones can be identified. In zone I (T=330–200 K), carrier concentration decreases by almost one order of magnitude. This behavior is expected due to thermal deactivation of deep levels presumably related to Cu, which at lower temperatures (or higher frequencies) stop contributing to the apparent carrier concentration. Depletion region width W increases by about three times, consistent with the decrease in N_a because $W \infty N_a^{-1/2}$. In zone II (T=200–110 K), W continues to increase, which indicates that ionized acceptor concentration in the region already depleted in zone I continues to decrease. At the same time, N_a remains mostly unchanged except for a slight increase in N_a. The slight increase of N_a at low temperature may be due to the spatial gradient of acceptors (which causes N_a to increase toward the back contact) overcoming the thermal deactivation mechanism (which causes N_a to decrease at low temperature). In zone IV ($T < 80$ K), W settles at a plateau, while N_a stays higher than 10^{16} cm^{-3}. It is evident that the entire absorber between CdS and the back-contact layer is depleted at the measurement frequency. Therefore, the value of depletion region at these temperatures and frequencies (5.45 μm in this case) is electrically active absorber thickness t. The value of N_a for zone IV qualitatively reflects the high space charge density at the back edge of the depletion region, which is now located in the highly conductive back-contact material (e.g., carbon paste) with high conductivity after moving out of the CdTe material. The absolute value of N_a, however, is not an accurate measurement of carrier concentration in the back-contact material since the device now resembles a metal–insulator–metal structure instead of an n$^+$–p junction. Therefore, the Mott–Schottky method to determine N_a is no longer applicable. Between zones II and IV lies zone III (T=110–80 K), where N_a experiences a sharp increase of two orders of magnitude and W also experiences a rapid increase. This is the transition zone between a partially depleted absorber (zone II) to a fully depleted absorber (zone IV). The change of N_a in zone III is in part contributed by the non-uniform distribution of N_a near the back contact, and therefore contains valuable information on the interface between CdTe and the back-contact material. An attempt to re-construct the spatial distribution of carrier concentration (i.e., N_a vs W) is premature at present since the numerical value of N_a is influenced by the freeze-out effect (i.e., the measured capacitance is with mixed contributions from the depletion capacitance due to the junction and the geometrical capacitance due to the absorber, which again renders the Mott–Schottky method invalid). For this reason, we take the carrier concentration N_a in zone II (just prior to the freeze out) for calculation of resistivity and mobility according to Eqs. (5) and (6), as shown below. It is worth noting that all three types of samples exhibit consistent freeze-out phenomena (i.e., zones III–IV), from which t and N_a can be reliably extracted. There is some distinct difference in zone I that is related to the deep levels introduced by Cu; details are given in Section 5.

We then inspect the admittance spectroscopy of these devices, i.e., frequency dependence of C and G/ω at a fixed temperature, as shown in Fig. 3. They agree well with the description by the equivalent circuit and derivation from there. The G/ω vs ω spectrum shows a peak at the inflection frequency ω_p. The C vs ω spectrum shows a step separating two plateaus: C_d at $\omega < \omega_p$ and C_g at $\omega > \omega_p$. Also plotted in Fig. 3 is the differential capacitance $\omega\, dC/d\omega$ vs ω spectrum. We identify ω_p from the negative peak in the $\omega\, dC/d\omega$ vs ω spectrum. In Fig. 4, we see that the bias dependence of the $\omega dC/d\omega$ vs ω spectrum satisfies the description by Eqs. (2)–(4). The square of ω_p exhibits a linear dependence on bias voltage as described by Eq. (4), from which a slope is extracted (Fig. 5). Using Eqs. (5) and (6), with measured values of t and N_a, we determine the resistivity of the film as $1.39 \times 10^7\ \Omega$ cm at T=100 K. Furthermore, we determine the mobility of the film as 1.96×10^{-3} cm^2/V/s. The results for all three samples are summarized in Table 1. In Fig. 6, we show the temperature dependence of W and N_a for all three types of devices.

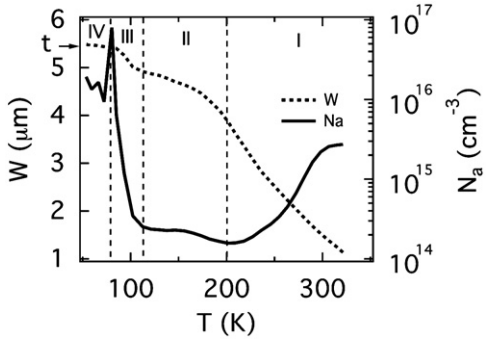

Fig. 2. Depletion region width W and carrier concentration N_a calculated at zero bias (measurement frequency 10 kHz) for a type A (Cu/NP) CdTe device are plotted against temperature. Four zones are identified in the temperature dependence of W and N_a, detailed descriptions of which are in the text.

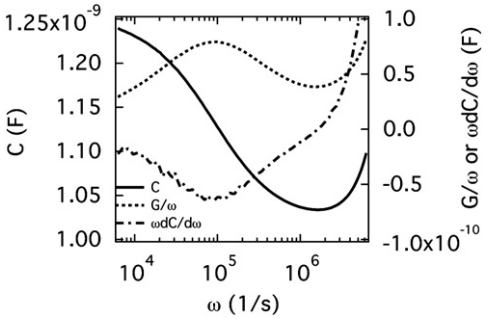

Fig. 3. Frequency dependence of capacitance C, normalized conductance G/ω, and normalized differential capacitance $\omega dC/d\omega$ taken at T=100 K from a type A (Cu/NP) CdTe solar cell with ~12% efficiency. All the curves agree well with the description of the equivalent-circuit model in Fig. 1.

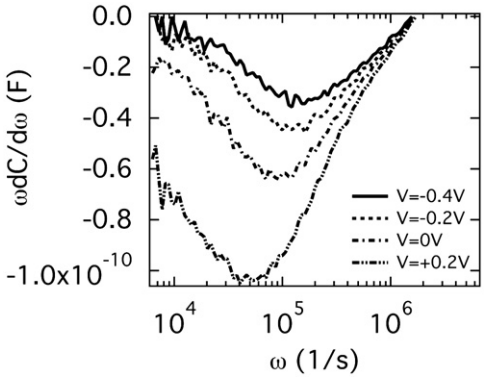

Fig. 4. Bias dependence of the normalized differential capacitance spectrum $\omega dC/d\omega$ vs ω. Data are taken from a type A (Cu/NP) device at $T=100$ K. As described by Eq. (4), the inflection frequency shows a redshift with increase in forward bias.

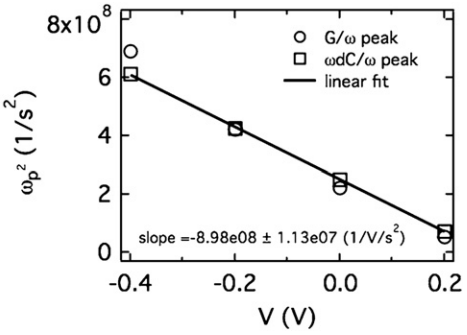

Fig. 5. Bias dependence of the square of inflection frequency ω_p^2 (squares), where ω_p is determined from $\omega dC/d\omega$ vs ω spectra shown in Fig. 4. A linear fitting (line) yields the slope used to determine ρ and μ according to Eqs. (5) and (6). Bias dependence of the squares of inflection frequency determined from conductance data (circles) is also shown.

Table 1
Summary of results for all three types of CdTe devices.

	Type A: Cu/NP	Type B: X/NP	Type C: X/X
t (μm)	5.45 ± 0.05	5.85 ± 0.05	7.95 ± 0.05
ρ (Ω cm)	1.39 ± 0.03e7	2.81 ± 0.06e7	1.89 ± 0.04e7
μ_h (cm^2/V/s)	1.96 ± 0.04e−3 $T=102$ K	1.1 ± 0.03e−3 $T=85$ K	1.0 ± 0.02e−3 $T=85$ K
E_{act} (meV)	154 ± 3	233 ± 8	129 ± 5
N_a (cm^{-3})	2.2e14	5.0e14	2.9e14

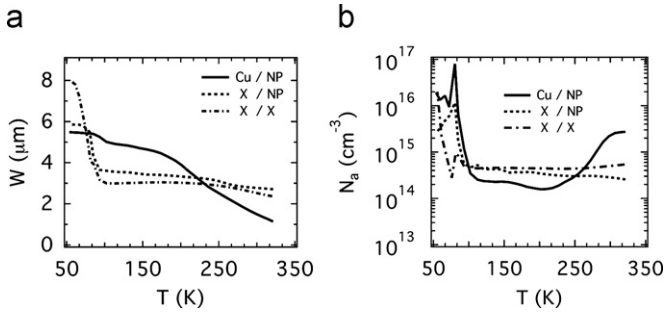

Fig. 6. Temperature dependence of depletion region width W (a) and carrier concentration N_a (b) for three types of CdTe solar cells with different back-contact formations. All three devices show similar freeze-out at low temperatures.

5. Discussion

The thicknesses (Table 1) of all three types of samples meet expectations from film growth and processing history and are explained well by understanding the back-contact formation illustrated in Fig. 7. The absorber thickness for type C (X/X) samples (7.95 μm) agrees well with the growth record, as no NP etching or Cu-containing back-contact material is used here. Measurements by a Dektak profilometer of the series of samples, performed immediately after the film growth, yield CdTe film thickness between 7.0 and 7.8 μm. This discrepancy is explained by the inherent non-uniformity of CdTe film across the device. This non-uniformity makes it difficult to directly compare the thickness measured by the capacitance method, which is for the entire contacted device, with those by other thickness measurements such as scanning electron microscope, which is at a specific location within the device. For the type B (X/NP) samples, absorber thickness drops drastically to 5.85 μm due to the NP etching, which is known to be a relatively strong etchant that not only reduces CdTe film thickness but also etches in between grains [4]. NP etching of CdTe also creates many Cd vacancies and leaves a Te-rich layer. The thickness of the Te layer identifiable in transmission electron microscopy is 0.1–0.2 μm [5]. The planar etching loss of CdTe (~0.1 μm) is expected to be far less than that of the preferential etching along the grain boundary, which can reach microns [4]. It is therefore very likely that electrically effective thickness in type B (X/NP) is the distance from the CdS layer to the bottom of the grain boundary, which is probably of high conductivity due to the relatively rich Te content [5]. Presumably, there is a transition region between the intact CdTe and the Te-rich layer. Details of the grain boundary effect and the transition region are the subject of further study. For the type A (Cu/NP) samples, absorber thickness further drops slightly to 5.45 μm. The significant amount of Cu [5] diffused from the back-contact paste possibly forms a CuTe alloy to reduce the measured absorber thickness and further takes the Cd vacancy sites to introduce deep levels. The existence of such deep levels is evident in the behavior of N_a and W in zone I, i.e., around room temperature. Such deep levels are noticeably absent in the type B (X/NP) and C (X/X) devices, as seen in zone I in Fig. 6(b), when Cu is not added to the carbon paste.

The peak that appears in the $\omega\, dC/d\omega$ vs ω spectrum exhibits typical thermal activation behavior. If one applies the conventional admittance spectroscopy analysis to this thermal activation phenomenon, the extracted activation energies for type A (Cu/NP), B (X/NP), and C (X/X) samples are 154 ± 3, 233 ± 7, and 129 ± 5 meV, respectively. This freeze-out activation energy reflects thermal activation of mobility [6] and carrier concentration of the majority carriers. Coincidently, these values are close

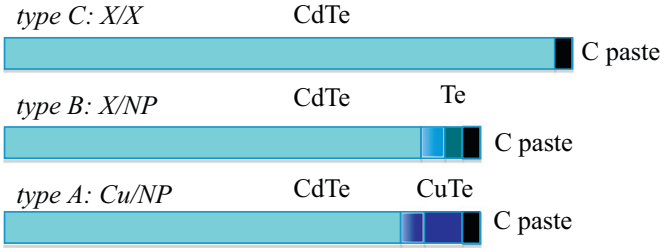

Fig. 7. Diagram showing absorber thickness for different back-contact formations in type A (Cu/NP), B (X/NP), and C (X/X) devices. The film thickness of the type A (Cu/NP) device (7.95 μm) agrees with the growth record and measurement by profilometer. The film thickness of the type B (X/NP) device (5.85 μm) indicates film loss due to NP etch and the formation of a Te-rich layer. The film thickness of the type C (X/X) device (5.45 μm) indicates alloying between Cu and Te and doping due to Cu in Cd vacancy.

to deep levels previously identified as H1 and H2 [7,8]. Furthermore, the voltage dependence of ω_p can easily be mistaken as a sign of trapping states that are spatially localized and energetically continuous, e.g., interface states, or as a result of the Frankel–Poole effect. Therefore, to avoid misinterpretation of freeze-out phenomenon as a deep-trap signature, we advise that future studies of admittance spectroscopy of thin film use correlated inspection of capacitance–voltage characteristics.

Obviously this method to measure thin-film thickness, resistivity, and mobility is not limited to CdTe material or to low-temperature measurements. It is also applicable to Cu(InGa)Se_2, amorphous silicon, and organic photovoltaic materials. In fact, it is applicable to any two-terminal semiconductor device that can be described by the equivalent-circuit model in Fig. 1, as long as inflection frequency (determined by resistivity, carrier concentration, mobility, and thickness) falls into the observable window of the measurement system given the frequency and temperature ranges. To measure materials with lower resistivity, e.g., CdTe film at room temperature, admittance spectroscopy and capacitance–voltage measurements must be performed at higher frequencies.

6. Conclusions

We have reported on a method developed upon coordinated admittance spectroscopy and capacitance–voltage techniques to measure resistivity, mobility, and absorber thickness in thin-film photovoltaic devices. The absorber thickness is measured by the depletion-region width at freeze-out temperatures at which the free carriers cease to respond to ac modulation. Based on a simple lumped-parameter equivalent-circuit model, we derive the inflection frequency at which admittance exhibits a step transition due to dielectric relaxation of the absorber. Resistivity—and, in turn, mobility—is determined from the bias dependence of the inflection frequency, knowing the absorber thickness and carrier concentration obtained by capacitance–voltage measurements. To demonstrate this method, we applied it to thin-film CdTe solar cells with back contacts formed under three different conditions: (A) with Cu after nitric–phosphoric etch, (B) without Cu after NP etch, and (C) neither Cu nor NP etch. The measured electrically active absorber thicknesses (5.45, 5.85, and 7.95 μm, respectively) agree well with growth and processing history and other methods. This method enables the retrieval of information on a number of issues related to the back-contact formation: the film loss due to NP etching, the formation of a Te-rich layer, the alloy of Cu and Te, and the deep level introduced by Cu in the back contact. We also investigate the underlying contributions by mobility and carrier concentration to thermal activation of the total freeze-out and caution against the possible erroneous interpretation as the previous labeled H1 and H2 deep levels.

Acknowledgements

The authors are grateful for insightful discussions with Dr. Yanfa Yan at the National Renewable Energy Laboratory, Dr. Jennifer Heath at Linfield College, and Dr. Oleg Sulima at GE Global Research. This research is supported by US Department of Energy Contract no. DE-AC36-08GO28308.

References

[1] J.D. Cohen, D.V. Lang, J.P. Harbison, A.M. Sergent, Photo-induced changes in the bulk density of gap states in hydrogenated amorphous silicon associated with the Staebler–Wronski effect, Solar Cells 9 (1983) 119–131.
[2] J.W. Lee, J.D. Cohen, W.N. Shararman, The determination of carrier mobilities in CIGS photovoltaic devices using high-frequency admittance measurements, Thin Solid Films 480–481 (2005) 336–340.
[3] D.H. Rose, F.S. Hasoon, R.G. Dhere, D.S. Albin, R.M. Ribelin, X.S. Li, Y. Mahathongdy, T.A. Gessert, P. Sheldon, Fabrication procedures and process sensitivities for CdS/CdTe solar cells, Prog. Photovolt. Res. Appl. 7 (1999) 331–340.
[4] X. Li, D.W. Niles, F.S. Hasoon, R.J. Matson, P. Sheldon, Effect of nitric–phosphoric acid etches on material properties and back-contact formation of CdTe-based solar cells, J. Vac. Sci. Technol. A 17 (1999) 805–809.
[5] D. Albin, R. Dhere, X. Wu, T. Gessert, M.J. Romero, Y. Yan, S. Asher, Perturbation of copper substitutional defect concentrations in CdS/CdTe heterojunction solar cell devices, Mater. Res. Soc. Symp. Proc. 719 (2002) 383–388.
[6] K. Suzuki, S. Seto, T. Sawada, K. Imai, Carrier transport properties of HPB CdZnTe and THM CdTe:Cl, IEEE Trans. Nucl. Sci. 49 (2002) 1287–1291.
[7] F.H. Seymour, V. Kaydanov, T.R. Ohno, Simulated admittance spectroscopy measurements of high concentration deep level defects in CdTe thin-film solar cells, J. Appl. Phys. 100 (2006) 033710-1–033710-5.
[8] J. Versluys, P. Clauws, P. Nollet, S. Degrave, M. Burgelman, DLTS and admittance measurements on CdS/CdTe solar cells, Thin Solid Films 431–432 (2003) 148–152.